AIAA JOURNAL
Vol. 37, No. 6, June 1999

# Seven-Hole Pressure Probe Calibration Method Utilizing Look-Up Error Tables

Christian W. Wenger* and William J. Devenport†
*Virginia Polytechnic Institute and State University, Blacksburg, Virginia 24061*

**A two-step calibration and measurement procedure for seven-hole pressure probes has been developed that allows simple and accurate real-time processing. The method adds an extra step to traditional least-squares calibration schemes such as Gallington's method (Gallington, R. W., "Measurement of Very Large Flow Angles with Non-Nulling Seven Hole Probes," *Proceedings of the 27th International Instrumentation Symposium*, Instrumentation Society of America, Triangle Park, NC, 1981, pp. 115–130) involving the interpolation of error look-up tables. A measurement system employing the two-step calibration scheme is described. Measurements are made in pipe and wind-tunnel flows, and a detailed uncertainty analysis is performed, to demonstrate the accuracy of the new scheme. Independent of the new scheme, the measurements also show some effects of Reynolds number, velocity gradient, and turbulence on the probe accuracy. The Reynolds number effect was not anticipated and may indicate the need for multiple calibrations in some circumstances.**

## I. Introduction

BECAUSE of their relative simplicity, seven-hole pressure probes are an attractive option for time-average, three-component flow velocity measurements. There are a number of possible geometries for a seven-hole probe,[1] the most common of which is the conical-ended probe shown in Fig. 1a. The probe tip contains seven pressure ports, one of which sits at the tip of the cone, with the remaining six arranged in a ring downstream. One of the chief advantages of the seven-hole probe (as compared with its five-hole cousin) is its ability to make acceptable measurements even at very large mean flow angles, typically up to 80 deg (Ref. 2). This is achieved by expressing the pressures sensed by the seven ports in terms of a series of pressure coefficients, the form of the coefficients depending on the angle of the flow.[2,3]

For low flow angles, the pressure measured by the center port is greater than those of the other six, and the pressures sensed by the probe are expressed in terms of the coefficients

$$c_\alpha = \frac{[(p_6 + p_7)/2] - [(p_4 + p_3)/2]}{p_1 - \bar{p}}, \qquad c_\beta = \frac{p_2 - p_5}{p_1 - \bar{p}} \tag{1}$$

where $\bar{p} = (p_2 + p_3 + p_4 + p_5 + p_6 + p_7)/6$ and $p_n$ is the pressure sensed by port $n$ (Fig. 1b). $C_\alpha$ and $C_\beta$ are designed to vary primarily with the pitch and yaw angles of the probe. They are used as the basis for calibrating the probe for actual pitch and yaw angles ($\alpha$ and $\beta$; Fig. 1c) and the relative total and static pressures ($p_t$ and $p_s$) expressed in terms of the coefficients

$$C_s^{(1)} = \frac{p_1 - p_s}{p_1 - \bar{p}}, \qquad C_t^{(1)} = \frac{p_1 - p_t}{p_1 - \bar{p}} \tag{2}$$

For high flow angles, for which the pressure measured by one of the surrounding ports is the greatest, the pressures sensed by the probe are expressed in terms of

$$C_\theta^{(i)} = \frac{p_i - p_1}{p_i - (p_{\mathrm{CW}} + p_{\mathrm{CCW}})/2}$$

$$C_\phi^{(i)} = \frac{p_{\mathrm{CW}} - p_{\mathrm{CCW}}}{p_i - (p_{\mathrm{CW}} + p_{\mathrm{CCW}})/2} \tag{3}$$

where $p_i$ is the pressure sensed by the port experiencing the greatest pressure, CW is the pressure port next to the $i$th pressure port in the clockwise direction, and CCW is the pressure port next to the $i$th pressure port in the counterclockwise direction in Fig. 1b. $C_\theta$ and $C_\phi$ are designed to vary primarily with the cone and roll angle of the probe and are used as the basis for calibrating the probe for actual cone and roll angle ($\theta$ and $\phi$; Fig. 1c) and the relative total and static pressures expressed in terms of the coefficients

$$C_s^{(i)} = \frac{p_i - p_s}{p_i - (p_{\mathrm{CW}} + p_{\mathrm{CCW}})/2}$$

$$C_t^{(i)} = \frac{p_i - p_t}{p_i - (p_{\mathrm{CW}} + p_{\mathrm{CCW}})/2} \tag{4}$$

Note that at high angles there are six different sets of pressure coefficients that may be used, depending on which port senses the greatest pressure.

With these coefficients defined, the task reduces to defining the functions

$$C_s^{(i)}(C_\theta, C_\phi), \quad C_t^{(i)}(C_\theta, C_\phi), \quad \theta^{(i)}(C_\theta, C_\phi), \quad \phi^{(i)}(C_\theta, C_\phi) \tag{5}$$

for each of the high-angle sectors and

$$C_s^{(1)}(C_\alpha, C_\beta), \quad C_t^{(1)}(C_\alpha, C_\beta), \quad \alpha(C_\alpha, C_\beta), \quad \beta(C_\alpha, C_\beta) \tag{6}$$

for the low-angle sector, in a form suitable for application as calibrations. There are a number of techniques to choose from. Among these are Gallington's[2] method, which involves fitting each of the functions to a two-dimensional polynomial by the method of least squares. Gallington's method assumes that the calibration functions are fairly smooth, and indeed it is our experience that this is the case. However, it is unable to account for deviations from the polynomial form and is, thus, not very accurate, the accuracy being typically ±1 deg for flow angles and ±2% for velocity magnitude. Zilliac[4] takes a different approach, fitting a piecewise quintic surface through the actual calibration points. Zilliac's method, although considerably more accurate (accuracies of ±0.5 deg for flow angles and ±1% for velocity magnitude), is significantly more difficult to implement on the irregularly sampled data of a calibration. It also ignores the smooth form of the calibration function, allowing for rapid local variations in the higher derivatives of the interpolation and, thus, some increased uncertainty when the measurement does not fall close to a calibration point. Other calibration methods include that due to Zeiger et al.,[1] which uses a purely local interpolation scheme on the calibration data itself, and that due to Vijayagopal and Rediniotis,[5] which uses a neural net approach.

The aim of this paper is to present the details of an alternative approach to the expression of the calibration functions that combines

Presented as Paper 98-0202 at the AIAA 36th Aerospace Sciences Meeting, Reno, NV, Jan. 12–15, 1998; received March 17, 1998; revision received Sept. 10, 1998; accepted for publication Sept. 12, 1998. 

*Graduate Research Assistant, Department of Aerospace and Ocean Engineering. Student Member AIAA.

†Associate Professor, Department of Aerospace and Ocean Engineering. Senior Member AIAA.

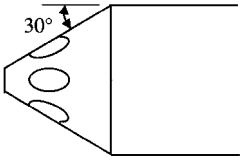


**Fig. 1a Conical probe tip and the pressure ports.**

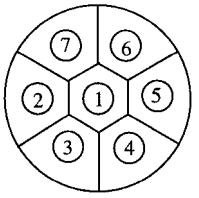


**Fig. 1b Tip divided into seven sectors, with each sector corresponding to a pressure port.**

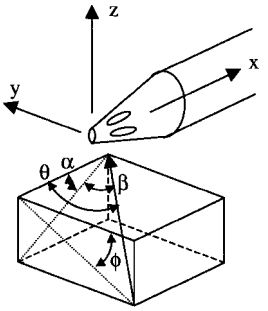


**Fig. 1c Flow angles pitch $\alpha$ and yaw $\beta$ used for low-angle measurements and cone $\theta$ and roll $\phi$ used for high-angle measurements.**

the simplicity of Gallington's method with the accuracy of fitting to the actual calibration points, as in Zilliac's technique. A measurement system employing this two-step calibration scheme is described. A detailed uncertainty analysis is performed to demonstrate the accuracy of the new scheme. As an application of the scheme, measurements are made in pipe and wind-tunnel flows to observe the behavior of seven-hole probes in turbulent flows with velocity gradient and in the presence of significant Reynolds number variations.

## II. Two-Step Calibration Method

The first step of the scheme involves fitting each of the calibration functions, Eqs. (5) and (6), with a global polynomial surface fit by the method of least squares, e.g., with a two-dimensional polynomial as in Gallington's method. In general, this surface will not go through all of the calibration points. If we denote the generic empirical calibration function as $C(C_a, C_b)$ and the polynomial surface fit as $f(C_a, C_b)$, then we write

$$C(C_a, C_b) = f(C_a, C_b) + e(C_a, C_b) \tag{7}$$

where $e(C_a, C_b)$ is the error in the surface fit at each of the calibration points. The second step simply involves the storage of $e(C_a, C_b)$ as a look-up table. During a measurement of $C_a$ and $C_b$, we use the global curve fit plus a simple interpolation of the error table to return an estimate of each calibrated value.

The rationale for a two-step process is that, by first applying a global surface fit to the data, we reduce the magnitude of the interpolated part and, thus, under certain circumstances, the magnitude of the interpolation error. This process offers no improvement if the global curve fit and local interpolation are of the same order. For example, if we use a cubic for the global fit, followed by a cubic spline for the local interpolation, we might as well use a cubic spline for the whole function. The advantage is in using global and local fits of different order. Because the calibration functions tend to be smooth, this implies that the higher-order derivatives vary only slowly across the calibration surface. It therefore makes sense to perform a high-order global surface fit that allows for this gradual variation, such as done by Gallington, and a low-order local interpolation, such as a linear one that allows for local variations only in the low-order derivatives. This minimizes the potential for error associated with oscillation in the interpolation function in between the calibration points. It is also considerably easier to implement on irregular data than a high-order piecewise interpolation.

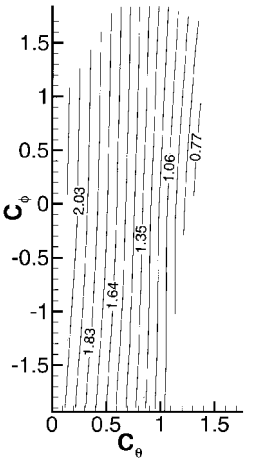


**Fig. 2 Static pressure coefficient as a function of cone- and roll-angle pressure coefficients for sector 3 (see Fig. 1b).**

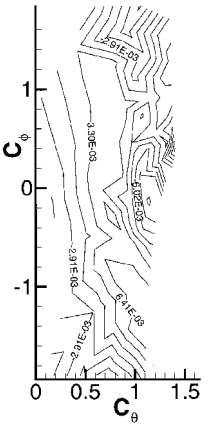


**Fig. 3 Error in the calibration curve fit of the static pressure coefficient as a function of cone- and roll-angle pressure coefficients for sector 3 (see Fig. 1b).**

As an example, Fig. 2 shows the function $C_s^{(3)}(C_\theta, C_\phi)$ (the empirical calibration function for the static pressure coefficient for high-angle sector 3) for our probe. Note the smooth form. Figure 3 shows the error $e(C_\theta, C_\phi)$ after a global cubic surface fit is calculated by the method of least squares and is subtracted from the data.

## III. Implementation

A seven-hole yaw probe measurement system was developed to perform time-average measurements in turbulent flows using the new calibration scheme. The probe used for this study, supplied by Aeroprobe Corporation, has a stem 15.2 cm in length and 2 mm in diameter. Within the stem are seven tubes, each of internal diameter 0.5 mm. The tip of the probe is machined in a conical shape (Fig. 1a), with a half-angle of 30 deg. The tubes in the stem are each fixed at the downstream end to short plastic tubes, which in turn can be attached to longer tubes that lead to pressure transducers.

An array of seven pressure transducers was constructed to read the seven probe pressures simultaneously. The array was designed to be small enough to be located in the wind tunnel without causing interference. Close proximity to the probe is desirable because the length of tubing connecting the probe to the transducers is minimized, and consequently, the settling time needed for statistically stationary measurements is minimized. The array is housed in a metal box of dimensions 18 × 10 × 5 cm, which is located approximately 1 m downstream of the probe during measurements.

During calibration the probe was mounted in an angle manipulator to place the probe at varying degrees of pitch and yaw. This manipulator places the tip of the probe on the axes of rotation. For the calibrations discussed in this paper, approximately 300 calibration points, spaced at intervals of 5 deg, were used.

To conduct the calibrations and subsequent flow condition studies, a fully developed turbulent pipe flow was used. The pipe flow, as described in detail by Shaffer,[6] has a 0.081-m diameter and 19.5-m length after a flow conditioning contraction, honeycomb, and screen. Hot-wire measurements performed by Wittmer et al.[7] demonstrate that the exit mean velocity profile of the pipe conforms to the $\frac{1}{7}$th power law[8] and that the Reynolds shear stress profile is linear and

in accord with the mean streamwise pressure gradient. For all calibrations and measurements, the probe tip was placed in the flow at the plane of exit.

Measurements were also performed in the empty test section of the Virginia Polytechnic Institute Stability Wind Tunnel. This is a large general-purpose facility with a test section $1.83 \times 1.83$ m in cross section and 7.32 m in length. Flow through the empty test section is closely uniform and of very low turbulence intensity (~0.05%) (Ref. 9).

The pressure transducers were manufactured by Data Instruments (Model XPCL04DTC). These transducers are specified to read from −4 to 4 in. of water (−1 to 1 kPa), and they are temperature compensated over a range of 0–50°C. The output voltage is generally from −25 to 25 mV and as such must be amplified to a suitable range for data acquisition. Therefore, each of the seven transducers was wired to a 100 gain instrumentation amplifier manufactured by Burr Brown (Model INA131AP). Finally, to reduce the noise in the signals, a low-pass filter with a cutoff frequency of 200 Hz was wired to the output of each amplifier.

The seven output signals from the transducer array are read using an eight-channel, sample and hold, multiplexer, 12-bit A/D board from Analogic (Model HSDAS-12). A personal computer with a 486 66-MHz processor is used to control the data acquisition, perform real-time data processing, and record the data. The data acquisition software, written in the C programming language specifically for the purpose of taking measurements with the seven-hole probe, allows the sampling frequency and number of samples to be selected as desired. For the purposes of this study, measurements were averaged over 3072 samples taken at 500 Hz.

## IV. Accuracy and Uncertainty

The accuracy of the two-step calibration scheme was assessed using the calibration measurements themselves. By removing a single measurement from this set, recomputing the calibration from the remainder, and then using this calibration to estimate the values at the missing point, the error associated with the curve fitting and interpolation procedures could be estimated at each calibration point. Because this procedure uses the calibration measurements at only half their true resolution, we estimate the true errors by dividing these estimates by 4 (relying on the fact that, to leading order, the error in a linear interpolation varies as the square of the distance between the points). Table 1 shows the average uncertainty (double the rms error) due to interpolation calculated using this method averaged over the low-angle sector and averaged over all of the high-angle sectors. The uncertainties, 0.003 deg for $\alpha$ and $\beta$ and 0.01% for velocity in the low-angle sector and 0.06 deg for $\alpha$, 0.03 deg for $\beta$, and 0.05% for velocity in all of the high-angle sectors, appear very small and (as will be shown subsequently) are insignificant when compared with the uncertainties associated with the rest of the measurement system. The flow angles, cone and roll, used for high-angle definitions have been converted to match the low-angle definitions, pitch and yaw, $\alpha$ and $\beta$.

**Table 1 Average uncertainties in pitch angle $\alpha$, yaw angle $\beta$, and total velocity $V$ and contributions arising from pressure transducer inaccuracy (trans), angle manipulator inaccuracy (manip), and interpolation inaccuracy (inter)**

| | Sector | |
|---|---|---|
| Uncertainty | Low | High |
| $\delta\alpha_{\text{total,deg}}$ | 0.35 | 0.42 |
| $\delta\alpha_{\text{trans,deg}}$ | 0.24 | 0.33 |
| $\delta\alpha_{\text{manip,deg}}$ | 0.25 | 0.25 |
| $\delta\alpha_{\text{inter,deg}}$ | 0.003 | 0.06 |
| $\delta\beta_{\text{total,deg}}$ | 0.33 | 0.36 |
| $\delta\beta_{\text{trans,deg}}$ | 0.20 | 0.26 |
| $\delta\beta_{\text{manip,deg}}$ | 0.25 | 0.25 |
| $\delta\beta_{\text{inter,deg}}$ | 0.003 | 0.03 |
| $\delta V_{\text{total,\%}}$ | 0.67 | 0.83 |
| $\delta V_{\text{trans,\%}}$ | 0.67 | 0.83 |
| $\delta V_{\text{manip,\%}}$ | 0 | 0 |
| $\delta V_{\text{inter,\%}}$ | 0.01 | 0.05 |

These errors were compared with those produced by the rest of the measurement system by means of a full uncertainty analysis. In addition to the interpolation factors, the uncertainty analysis included the inherent uncertainty associated with the pressure transducers, estimated to be ±0.005 in. of water (±1.2 Pa), at 20:1 odds, and the uncertainty in the reading of the flow angles from the angle manipulator used during the calibration, ±0.25 deg. Uncertainties were combined according to the root-sum square technique of Kline and McClintock,[10] the required partial derivatives, where necessary, being determined numerically from the calibration data.

Because the uncertainties are dependent on the slopes of the calibration curves, they are functions of the flow angles. Therefore, the uncertainties were averaged over the range of flow angles (actually mean-square averaged). Because measurements falling in the low- and high-angle sectors involve different sets of calculations, the uncertainties for the two regimes were treated separately. The average uncertainties in both the low-angle sector and all of the high-angle sectors together are given in Table 1. The high-angle measurements go up to cone angles of approximately 45 deg.

Table 1 also shows the separate contributions to these uncertainties arising from the pressure transducer accuracy (which clearly dominates the velocity uncertainty) from the angle manipulator accuracy (which dominates the measured angle uncertainties). Most notably, we see that the two-step calibration procedure used is sufficiently accurate to be a negligible part of the total uncertainty for all quantities.

## V. Test Measurements

The new calibration scheme was applied to measurements made in pipe and wind-tunnel flows to observe the behavior of seven-hole probes in turbulent flows with velocity gradient and in the presence of significant Reynolds number variations.

Two calibrations and two velocity profile measurements were performed at the exit of the fully developed turbulent pipe flow already described. The first calibration and profile were measured at a Reynolds number of $2.52 \times 10^3$ based on the diameter of the probe, the pipe Reynolds number being $1.0 \times 10^5$. The calibration was performed on the centerline of the flow, where the turbulence intensity was 3% and the velocity gradient zero. The second calibration and profile were measured in the same way but at a probe Reynolds number of $3.9 \times 10^3$. Both velocity profiles were processed with both calibrations.

Figure 4 shows the results of the first velocity profile measurement ($Re = 2.52 \times 10^3$) processed using both calibrations. The results of both calibrations are profiles consistent with the $\frac{1}{7}$th power law profile, but the second calibration underestimates the $u$ velocity component everywhere by about 1% and produces a slightly shifted $w$ component. Note that the $v$ and $w$ velocity profiles do not converge

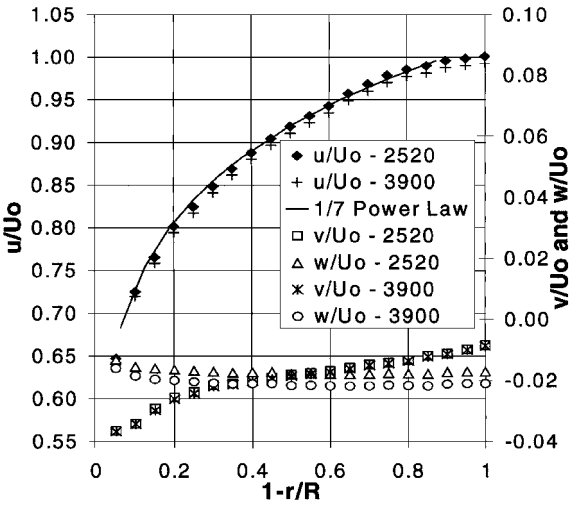


**Fig. 4 Mean velocity profile of all three components measured with the seven-hole pressure probe at Reynolds number $2.52 \times 10^3$ (based on the diameter of the probe): results for both calibrations at Reynolds numbers $2.52 \times 10^3$ and $3.9 \times 10^3$ as indicated in the legend.**

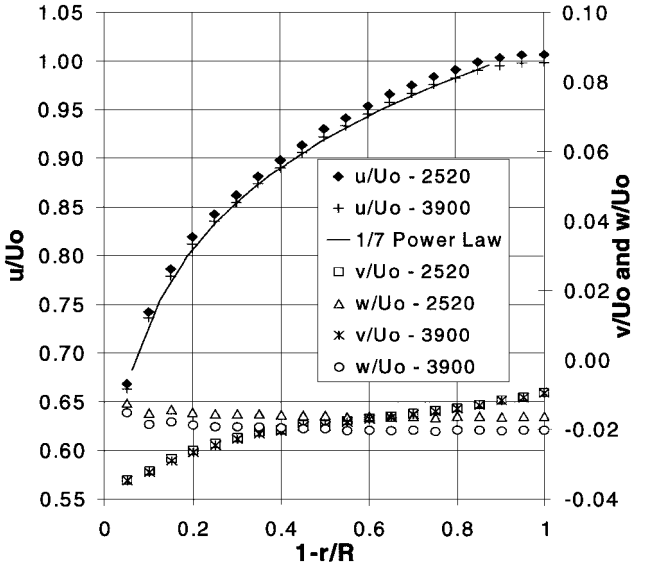


**Fig. 5 Mean velocity profile of all three components measured with the seven-hole pressure probe at a Reynolds number of $3.9 \times 10^3$ (based on the diameter of the probe): results for both calibrations at Reynolds numbers of $2.52 \times 10^3$ and $3.9 \times 10^3$ as indicated in the legend.**

to zero at the center of the flow because of an angle of about 1 deg between the probe axis and that of the pipe present during the measurements. Processing the second velocity profile ($Re = 3.9 \times 10^3$) with both calibrations produced complementary results (Fig. 5), the high-Reynolds-numbercalibration producing the correct profile but the low-Reynolds-numbercalibration overestimating $u$ by about 1% at all stations.

The difference between the results produced by the two calibrations suggests a Reynolds number effect on the yaw-probe calibration. Reynolds number effects on pitot-probe measurements are generally thought to become significant for Reynolds numbers based on the tube diameter of less than about 1000 (Ref. 11). The presence of a Reynolds number effect with the present probe, therefore, is not surprising, given that the Reynolds number based on the diameter of the individual tubes is one-quarter of the values earlier stated. However, because not much attention has been given to Reynolds number issues in seven-hole probe measurements, this effect was considered worthy of further investigation.

A sequence of four sets of measurements was made to this end. The probe was placed at zero angle, and the coefficient

$$C_s = \frac{p_1 - p_s}{p_1 - \bar{p}}$$

was measured as a function of probe Reynolds number. If the probe calibration were Reynolds number independent, this parameter would not vary. Three such sets of measurements were made in the turbulent pipe flow, two with the probe mounted in the angle manipulator used during calibration and one with the probe supported by a much smaller, more aerodynamic mount. One set of measurements was also made with the probe mounted in the center of the $1.83 \times 1.83$ m section of the Virginia Polytechnic Institute Stability Wind Tunnel test section. For the pipe-flow measurements (which were made at the pipe exit), the static pressure $p_s$ was taken as atmospheric. For the stability tunnel measurements, the static pressure was monitored using the wind-tunnel reference pitot-static probe, located a short distance upstream and to one side of the yaw probe. Tests were made using the different configurations and facilities to be certain that the effects observed could not be ascribed to blockage or other facility-dependent effects. The measurements (Fig. 6) clearly show a consistent Reynolds number effect that remains significant at least to a probe Reynolds number of $8 \times 10^3$. Measurements made in the turbulent pipe flow with the probe pitched and yawed (Fig. 6) show that this effect is not confined to low-angle measurements.

Clearly this Reynolds number effect places limits on the accuracy of this probe without the use of multiple calibrations covering

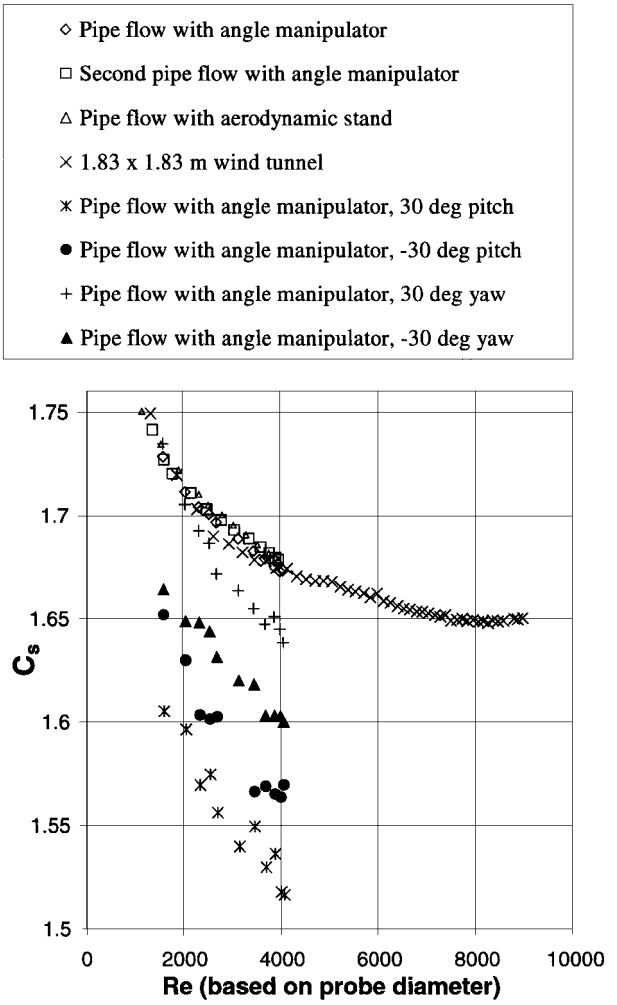


**Fig. 6 Variation of $C_s$ with respect to flow speed for several measurements done with various facilities.**

a range of Reynolds numbers or the development of a correction scheme. (The systematic variation of the data in Fig. 6 suggests that this may be feasible.) For our applications (high-Reynolds-number wind-tunnel studies with the present probe) the effects of Reynolds number are sufficiently small that we plan to ignore them and accept the increased uncertainty. This may not be possible using some of the very small probes that are currently under development at other laboratories.[5]

The pipe flow velocity profiles also suggest the influences of other flow conditions, such as turbulence and velocity gradient, on the yaw probe measurements. Chue[11] compiled the results of several investigations of pitot-static probe measurement errors due to velocity gradients. The conclusions presented from those studies suggest that the displacement of the effective probe center from the geometric center toward the direction of higher velocity tends to be only 10–16% of the outer diameter of the probe. In this case, that would be a distance of approximately 0.32 mm, which is roughly the same as the uncertainty in the position of the probe for these measurements. The variation of the $v$ velocity component near the wall also could be caused by the velocity gradient because one would expect it to produce a difference between the pressure sensed by the upper and lower pressure ports.

The discrepancies in the measurements near the wall could also be due to turbulence effects. The turbulence intensity increases to ~20% in the vicinity of the pipe wall. Results of studies concerning these errors, compiled by Chue,[11] demonstrated that turbulence intensities of 20% can cause errors of approximately 1% in velocity measurements. Therefore, we might expect the turbulence to cause only modest deviations from the theoretical. Another factor to consider at locations near the wall is blockage, which could also

be responsible for the differences between the true and measured velocities at those locations.

Considering the number of factors that can cause inaccurate measurements near the pipe wall, judgments as to the reason for the deviations from the true velocities are uncertain. However, an important conclusion can still be drawn, and that is that the velocity gradient and turbulence intensity increases did not drastically affect the accuracy of the measurements. The measurements all lie within approximately 2% of the theoretical $\frac{1}{7}$th power law profile even at the locations nearest to the wall. This result is very encouraging in that the calibrations seem robust enough to provide accurate measurements in a variety of flow conditions, which is exactly what is needed in a measurement system for use in turbulent flows.

## VI. Conclusions

A simple, accurate two-step calibration method for seven-hole pressure probes has been introduced. The calibration method involves an initial least-squares curve fit of the calibration data using a higher-order polynomial to represent the smooth trend of the calibration data. In the second step, error tables are constructed by comparing the calibration data to the least-squares curve fit. Then, during a measurement, the error in the curve fit is found by a low-order interpolation of the error tables. This method provides an exact match to the calibration data, while avoiding possible unwanted fluctuations of high-order local polynomial interpolations.

A measurement system employing the two-step calibration scheme was developed. Analysis of the uncertainties showed that the pressure-transducer inaccuracy dominates the overall uncertainty of the velocity measurement and that the uncertainty of the angle manipulator used during calibration dominates the overall uncertainty of the angle measurements. The uncertainty associated with the two-step calibration was shown to be negligible.

The new calibration scheme was applied to measurements made in pipe and wind-tunnel flows to observe the behavior of seven-hole probes in turbulent flows with velocity gradient and in the presence of significant Reynolds number variations. The measurements clearly show a consistent Reynolds number effect that remains significant at least to a probe Reynolds number of $8 \times 10^3$. Measurements made in the turbulent pipe flow with the probe pitched and yawed show that this effect is not confined to low-angle measurements. Without the use of multiple calibrations covering a range of Reynolds numbers, this Reynolds number effect places limits on the accuracy of the probe. High-velocity gradient, blockage, and turbulence intensity did not greatly increase the inaccuracies in the measurements. In general, the pressure probe measurement system proved to be a suitable tool for taking time-average measurements in flows with widely varying conditions, e.g., turbulent flows.

## Acknowledgments

The authors would like to thank the members of the Office of Naval Research, in particular L. Patrick Purtell, for their support under Awards N00014-94-1-0744 and N00014-96-1-0970.

## References

[1]Zeiger, M. D., Chalmeta, L. P., and Telionis, D. P., "Tip Geometry Effects on Calibration and Performance of Seven-Hole Probes," AIAA Paper 98-2810, June 1998.

[2]Gallington, R. W., "Measurement of Very Large Flow Angles with Non-Nulling Seven Hole Probes," *Proceedings of the 27th International Instrumentation Symposium*, Instrumentation Society of America, Triangle Park, NC, 1981, pp. 115–130.

[3]Bryer, D. W., and Pankhurst, R. C., *Pressure-Probe Methods for Determining Wind Speed and Flow Direction*, Her Majesty's Stationery Office, London, 1971, pp. 1–50.

[4]Zilliac, G. G., "Modeling, Calibration, and Error Analysis of 7-Hole Pressure Probes," *Experiments in Fluids*, Vol. 14, No. 1/2, 1993, pp. 104–120.

[5]Vijayagopal, R., and Rediniotis, O., "Miniature Multi-Hole Pressure Probes: Their Neural Network Calibration and Frequency Response Enhancement," AIAA Paper 98-0204, Jan. 1998.

[6]Shaffer, D. M., "Reynolds Stress Measurement Downstream of a Turbine Cascade," M.S. Thesis, Dept. of Mechanical Engineering, Virginia Polytechnic Inst. and State Univ., Blacksburg, VA, Aug. 1985.

[7]Wittmer, K. S., Devenport, W. J., and Zsoldos, J. S., "A Four-Sensor Hot-Wire System for Three-Component Velocity Measurement," *Experiments in Fluids*, Vol. 24, No. 5/6, 1998, pp. 416–423.

[8]Cheremisinoff, N. P., *Fluid Flow: Pumps, Pipes and Channels*, Ann Arbor Science, Ann Arbor, MI, 1981, p. 95.

[9]Choi, K., and Simpson, R., "Some Mean Velocity, Turbulence, and Unsteadiness Characteristics of the VPI and SU Stability Wind Tunnel," Dept. of Aerospace and Ocean Engineering, Rept. VPI-AOE-161, Virginia Polytechnic Inst. and State Univ., Blacksburg, VA, Dec. 1987.

[10]Kline, S. J., and McClintock, F. A., "Describing Uncertainties in Single Sample Experiments," *Mechanical Engineering*, Vol. 75, No. 1, 1953, p. 3.

[11]Chue, S. H., "Pressure Probes for Fluid Measurement," *Progress in Aerospace Sciences*, Vol. 16, No. 2, 1975, pp. 147–223.

R. P. Lucht
*Associate Editor*